International Journal of Dental Sciences and Research, 2020, Vol. 8, No. 1, 7-16
Available online at http://pubs.sciepub.com/ijdsr/8/1/2
Published by Science and Education Publishing
DOI:10.12691/ijdsr-8-1-2

Surface Registration Accuracy of Clinically Obtained Intraoral Optical Scans with Manually Threshold Segmented CBCT Data

Krzysztof Andruch*, Mariusz Malecki*

Department of Dental Prosthetic, Medical University of Lodz, Poland
*Corresponding author: andruchk@wp.pl, mariuszmalecki1@gmail.com

Received October 04, 2019; Revised November 11, 2019; Accepted November 18, 2019

Abstract Combining CBCT imaging and intraoral scans with an intention to prepare comprehensive treatment plans is common in clinical practice. Segmentation and superimposition of models is indispensable when planning complicated prosthetic reconstructions. The authors of this publication evaluated registration discrepancies of virtual dental arch models obtained by means of CBCT imaging at different segmentation thresholds with intraoral dental scans. For comparisons, intraoral digital scans and volumetric CBCT scans of the upper and lower jaw were used in randomly selected patients. The mean distance, Gaussian mean and standard deviation from the Gaussian mean as registration inconsistencies between the combined models were measured and subjected to a statistical analysis. The results showed that the registration of superimposed models may be affected by errors of up to 300 microns in the case of full dental arches. The statistical analysis proved that there was no correlation between the segmentation threshold and the quantitative variables studied (e.g. mean distance, Gaussian mean and standard deviation from the Gaussian mean). The results of this study indicate that CBCT data and full arch optical scans can be superimposed and successfully applied under clinical conditions within the accepted error.

Keywords: *CBCT threshold segmentation, intraoral full arch scan, STL registration accuracy*

Cite This Article: Krzysztof Andruch, and Mariusz Malecki, "Surface Registration Accuracy of Clinically Obtained Intraoral Optical Scans with Manually Threshold Segmented CBCT Data." *International Journal of Dental Sciences and Research*, vol. 8, no. 1 (2020): 7-16. doi: 10.12691/ijdsr-8-1-2.

1. Introduction

The combination of CBCT imaging with virtual models obtained with the use of an intraoral scanner enables the design and implementation of complex therapeutic plans combining aesthetic, surgical, prosthetic, implantological, orthodontic and orthognathic aspects of treatment. The diagnostic accuracy of cone beam computed tomography has been analysed in many studies [1,2,3]. Virtual models obtained through segmentation from CBCT are used in procedures combining surgery, prosthetics, implantology and other dental specialties [4,5,6]. Segmentation allows to extract any anatomical structures (teeth, bones) and save them as STL files due to differences in the gray level of the acquired x-ray image. Segmentation can be performed manually, semi-automatically or automatically [7,8]. It has been proven that segmentation quality is affected mainly by CBCT image quality (voxel size, contrast dynamics – thanks to 14-bit gray level depth), the presence of artefacts (caused by prosthetic restorations on a metal or zirconium dioxide substructure), patient's position stability during the process of acquisition and experience of the operator performing manual segmentation [9,10]. An uncomplicated and commonly used method of manual segmentation is the single threshold value. It allows for easy segmentation of radiologically dense structures such as tooth enamel or cortical lamina. Changes in the segmentation threshold affect the geometric fidelity of segmented surfaces. Manual segmentation has also been shown to be more accurate than semi-automatic segmentation [11,12,13].

Intraoral scans allow to eliminate plaster models and simplify communication with the dental laboratory. In addition, they digitize the design process and improve the accuracy of restorations. Currently, they enable the production of all types of prosthetic restorations, i.e. inlays, onlays, crowns, bridges, implant-supported restorations and also removable dentures [14,15]. New scanners allow to create virtual models with an accuracy of 15-50 microns, which is sufficient to delineate a tooth finishing line [16,17,18].

Registration accuracy of dental arches has a fundamental impact on the precision of the therapeutic process and has been the subject of few reports [19,20]. The interest in this aspect is important as it determines the effectiveness of treatment and influences the clinical course of applied procedures, which is exemplified by the use of surgical guides for dental implant positioning [21,22].

The aim of this study was to evaluate discrepancies in the registration of virtual dental arch models obtained

through CBCT imaging at various thresholds of segmentation with an intraoral digital scan.

2. Materials and Methods

Volumetric digital CBCT scans of the upper and lower dental arches in 15 randomly selected patients (4 males and 11 females) were used for comparisons. The material included 14 scans of the maxilla and 13 scans of the mandible, 14 of which were performed with the use of Vatech Pax-I 3d Green Corea (using the following parameters: 14.35 dGy/cm2, 8[mA], 94 [kVp]) and one with PaxReve3d Corea (13.24 dGy/cm2, 8[mA], 97[kVp]) in disclusion between arches using a standard bite stick. The data obtained in DICOM (Digital Imaging & Communication in Medicine) format were processed in Ez3DPlus software (E-Wootech, Seoul, Republic of Korea) using manual geometric segmentation, which was carried out first to separate maxilla and mandible and then to isolate only the crowns of teeth (chewing surfaces, incisal edges and side walls to the cementoenamel junction). Using the tool for single threshold segmentation (at four different arbitrarily selected levels), four STL files of the same dental arch were obtained. The selection of four different segmentation thresholds was dictated by an attempt to extract the best image of the dental surface for further comparisons and was based on the visual evaluation of the images according to the following scheme.

The first threshold was assigned when the soft tissue artefacts disappeared; the fourth just before the occurrence of defects in the segmented surfaces of dental crowns, while the second and third were optimized with a visual assessment (Figure 1). Segmentation of all models was carried out by the same person. The digital model was made with the use of Cerec Ac intraoral scanner with Omnicam camera (Sirona, Germany) and the scans were performed by the same person with the same parameters, according to one chosen strategy. The scanner was calibrated before each scanning procedure and the generated models of the maxilla and the mandible were saved in STL format. All STL files obtained from CBCT and the optical scanner were subjected to preparatory processing, which involved the removal of artefacts and cutting out of the unwanted part to the cementoenamel junction using Meshmixer.

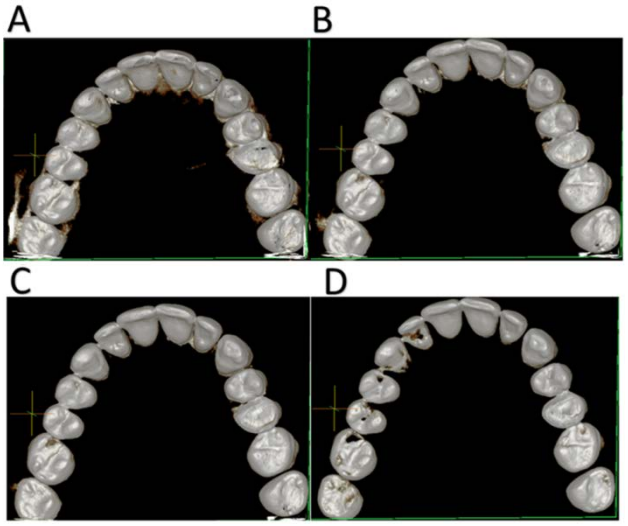

Figure 1. Example of the four different CBCT segmentation thresholds (Ez3DPlus software) : A – first threshold, B – second threshold, C – third threshold, D – fourth threshold.

The STL models obtained from CBCT were superimposed on the STL optical reference model using Cloud Compare (CC) (3D point cloud and mesh processing software Open Source Project). Superimposition of the models and an error analysis were performed using ICP (Iterative Closest Point) algorithm. Such a procedure allowed obtaining mean distance, Gaussian mean and standard deviation from the Gaussian mean between point clouds of the superimposed surfaces (Figure 2). During the first stage, the two models were superimposed manually, guided by a visual evaluation to fit together accurately. Next, automatic registration was performed based on the ICP algorithm. After that, the outermost parts were cut off and the models were registered again, which allowed to selectively remove contact points as areas inaccessible for optical scanning. Finally, the models were registered again and triangular grids were transformed into a cloud of 1,000,000 points for each model, which made the calculations possible (Figure 3). Results were collected as screenshots and recorded in (Table 1).

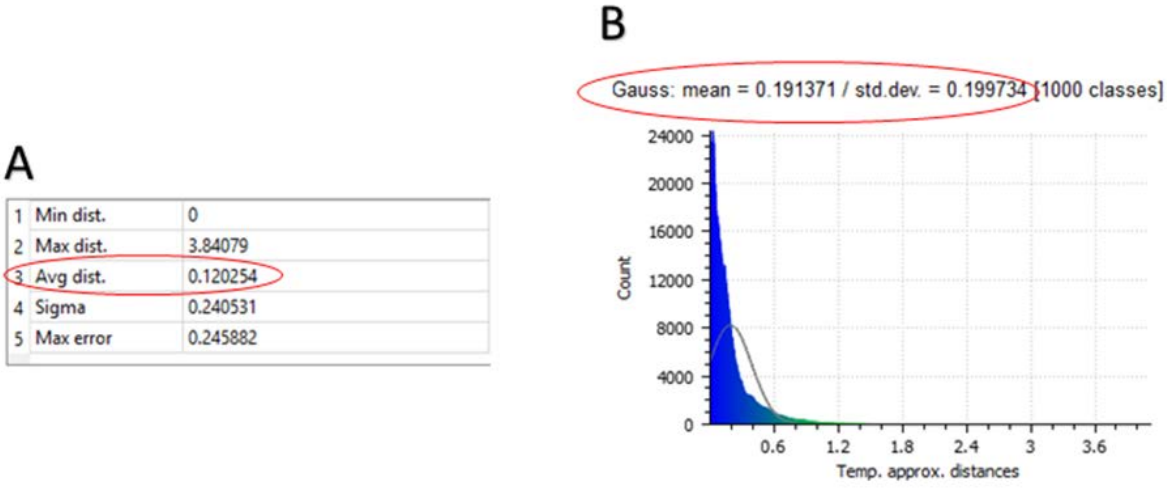

Figure 2. Sample results of statistical calculations from CloudCompare collected in the form of screenshots: A – table from which the mean distance between clouds of the examined models was read, B – graph from which the Gaussian mean and standard deviation were read

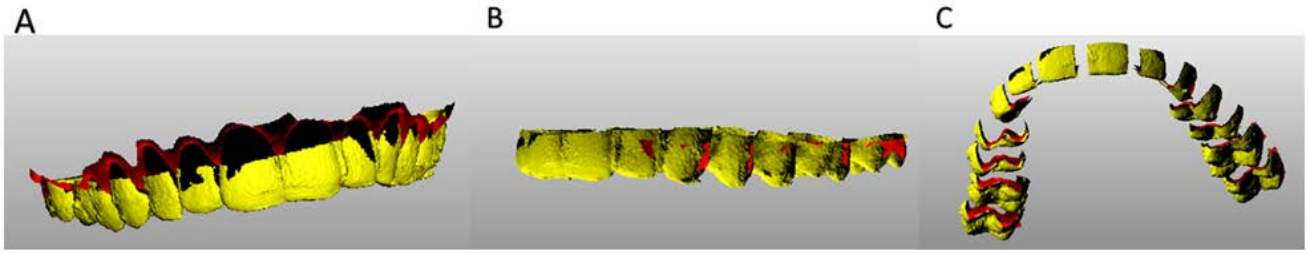

Figure 3. The process of superimposing the model segmented from CBCT (yellow) onto the reference model obtained from the optical scan (red). A – first manual registration of the models; B – models cut off after automatic registration; C – models with contact points removed after subsequent automatic registration

Table 1. Results of mean distance, Gaussian mean and standard deviation from the Gaussian mean for all the examined cases

Cases	**CBCT segmentation thresholds**			
	1	2	3	4
1	886	1008	1060	1200
AV Dist	0,194	0,182	0,224	0,106
Gauss SD	0,36	0,372	0,404	0,219
Gauss mean	0,294	0,28	0,32	0,192
2	1070	1220	1300	1520
AV Dist	0,108	0,147	0,205	0,346
Gauss SD	0,201	0,339	0,392	0,316
Gauss mean	0,19	0,227	0,285	0,453
3	1000	1200	1420	1600
AV Dist	0,295	0,176	0,152	0,164
Gauss SD	0,42	0,22	0,206	0,224
Gauss mean	0,395	0,265	0,239	0,251
4	1010	1234	1410	1606
AV Dist	0,413	0,425	0,277	0,544
Gauss SD	0,543	0,545	0,376	0,548
Gauss mean	0,51	0,515	0,366	0,643
5	1000	1100	1230	1410
AV Dist	0,238	0,19	0,12	0,103
Gauss SD	0,381	0,358	0,199	0,249
Gauss mean	0,329	0,268	0,191	0,181
6	1000	1110	1246	1310
AV Dist	0,265	0,244	0,252	0,152
Gauss SD	0,38	0,383	0,408	0,253
Gauss mean	0,349	0,339	0,343	0,238
7	1170	1280	1420	1586
AV Dist	0,308	0,286	0,263	0,316
Gauss SD	0,43	0,396	0,384	0,415
Gauss mean	0,395	0,371	0,352	0,401
8	1302	1488	1600	1718
AV Dist	0,289	0,298	0,317	0,388
Gauss SD	0,444	0,459	0,449	0,526
Gauss mean	0,381	0,398	0,41	0,485
9	764	900	1050	1204
AV Dist	0,256	0,082	0,069	0,056
Gauss SD	0,502	0,268	0,227	0,197
Gauss mean	0,342	0,16	0,132	0,124

10	762	952	1100	1224
AV Dist	0,127	0,1004	0,102	0,162
Gauss SD	0,294	0,196	0,235	0,355
Gauss mean	0,2	0,171	0,178	0,241
11	1000	1200	1400	1600
AV Dist	0,181	0,155	0,135	0,131
Gauss SD	0,347	0,252	0,243	0,211
Gauss mean	0,276	0,245	0,22	0,209
12	1094	1218	1410	1602
AV Dist	0,243	0,174	0,201	0,198
Gauss SD	0,362	0,264	0,326	0,301
Gauss mean	0,343	0,259	0,292	0,284
13	1100	1250	1320	1520
AV Dist	0,171	0,323	0,137	0,086
Gauss SD	0,294	0,517	0,287	0,176
Gauss mean	0,249	0,424	0,216	0,166
14	1170	1300	1500	1602
AV Dist	0,191	0,208	0,161	0,154
Gauss SD	0,338	0,315	0,273	0,234
Gauss mean	0,281	0,292	0,236	0,228
15	1020	1200	1490	1688
AV Dist	0,095	0,079	0,042	0,049
Gauss SD	0,164	0,154	0,098	0,106
Gauss mean	0,177	0,156	0,103	0,124
16	1000	1310	1650	1948
AV Dist	0,143	0,115	0,109	0,116
Gauss SD	0,183	0,155	0,145	0,2005
Gauss mean	0,236	0,205	0,191	0,198
17	980	1050	1300	1460
AV Dist	0,205	0,179	0,125	0,189
Gauss SD	0,421	0,352	0,262	0,344
Gauss mean	0,29	0,269	0,205	0,269
18	1050	1270	1450	1606
AV Dist	0,139	0,118	0,089	0,158
Gauss SD	0,233	0,268	0,174	0,292
Gauss mean	0,226	0,203	0,167	0,245
19	1050	1300	1470	1550
AV Dist	0,17	0,123	0,106	0,28
Gauss SD	0,268	0,21	0,264	0,427
Gauss mean	0,245	0,194	0,181	0,368
20	1010	1220	1350	1500
AV Dist	0,208	0,125	0,115	0,185
Gauss SD	0,332	0,198	0,201	0,253
Gauss mean	0,296	0,195	0,193	0,27
21	1062	1400	1512	1666
AV Dist	0,431	0,285	0,329	0,372
Gauss SD	0,519	0,376	0,413	0,46
Gauss mean	0,528	0,382	0,42	0,473

22	1050	1204	1302	1400
AV Dist	0,288	0,119	0,266	0,31
Gauss SD	0,413	0,317	0,42	0,498
Gauss mean	0,379	0,251	0,355	0,402
23	1000	1200	1400	1610
AV Dist	0,203	0,178	0,154	0,1666
Gauss SD	0,362	0,315	0,293	0,325
Gauss mean	0,288	0,263	0,241	0,261
24	1150	1390	1520	1600
AV Dist	0,104	0,041	0,075	0,058
Gauss SD	0,231	0,094	0,199	0,132
Gauss mean	0,173	0,106	0,14	0,119
25	920	1280	1470	1600
AV Dist	0,564	0,484	0,349	0,676
Gauss SD	0,566	0,469	0,335	0,688
Gauss mean	0,675	0,58	0,429	0,787
26	1080	1200	1370	1440
AV Dist	0,34	0,292	0,437	0,43
Gauss SD	0,484	0,402	0,519	0,351
Gauss mean	0,448	0,386	0,551	0,541
27	1200	1300	1400	1560
AV Dist	0,216	0,259	0,211	0,174
Gauss SD	0,329	0,343	0,292	0,236
Gauss mean	0,315	0,357	0,31	0,262

3. Results

These values were subjected to a statistical analysis. In the first step, basic descriptive statistics of the quantitative variables were calculated to check the normal distribution of these variables using TIBCO Statistica 13.3. This test showed that the distribution of the variables, i.e. the segmentation threshold and standard deviation from the Gaussian mean, did not differ significantly from the normal distribution. A different situation was observed for the mean distance and the Gaussian mean. Therefore, skewness was analysed. Since its absolute value did not exceed 2, it was assumed that the distribution was similar to the normal distribution [23]. Such a situation was observed in the case of all the quantitative variables examined in the study, which allowed the authors to conclude that the investigated distributions were not significantly asymmetrical with respect to the mean value. The Shapiro-Wilk test was applied to check whether the assumptions for the parametric tests were met. The Student's t-test was selected for one sample with the significance level totalling alpha=0.05 per each variable (Table 2).

In order to check the compatibility between the optical scan image and the CBCT image, several Student's t-tests were performed for one sample. The mean for the tested sample was calculated with reference to compliance parameters (mean distance, Gaussian mean and standard deviation from the Gaussian mean) together with 95% confidence interval (CI) for the mean. The values obtained were compared with the 0 value, which represented perfect compliance between both images. The results recorded were statistically significant for all the three parameters. In the case of the mean distance, a statistically significant result was obtained: $t(107) = 18.55$; $p < 0.001$, which means that the mean distance observed in the study (0.21) was statistically significantly higher than the 0 value. The confidence interval (95%) for the mean was within the limits of 0.19 – 0.23, hence the mean distance value obtained was statistically significantly higher than 0.19 and statistically lower than 0.23. Consequently, a statistically significant result was also obtained for the Gaussian mean, i.e. $t(107) = 24.44$; $p < 0.001$, where the confidence interval of 95% was within the limits of 0.27 – 0.32. Similarly, in the case of standard deviation from the Gaussian mean, the results obtained were as follows: $t(107) = 28.62$; $p < 0.001$, which means that the value of standard deviation from the Gaussian mean was statistically significantly higher than 0.30 and statistically significantly lower than 0.35 (Figure 4).

Table 2. Basic descriptive statistics of the examined quantitative variables

	M	*Me*	*Min*	*Max*	*SD*	*Sk.*	*Kurt.*	*W*	*p*
segmentation threshold	1288.56	1290.00	762.00	1948.00	232.31	0.09	-0.48	0.982	0.153
mean distance	0.21	0.18	0.04	0.68	0.12	1.26	2.00	0.912	<0.001
Gaussian standard deviation	0.32	0.32	0.09	0.69	0.12	0.38	-0.13	0.983	0.188
Gaussian mean	0.30	0.27	0.10	0.79	0.13	1.17	1.79	0.925	<0.001

M – mean; Me – median; Min and Max – lowest and highest distribution value; SD – standard deviation; Sk. – skewness; Kurt. – kurtosis; W – result of the Shapiro-Wilk test; p – statistical significance.

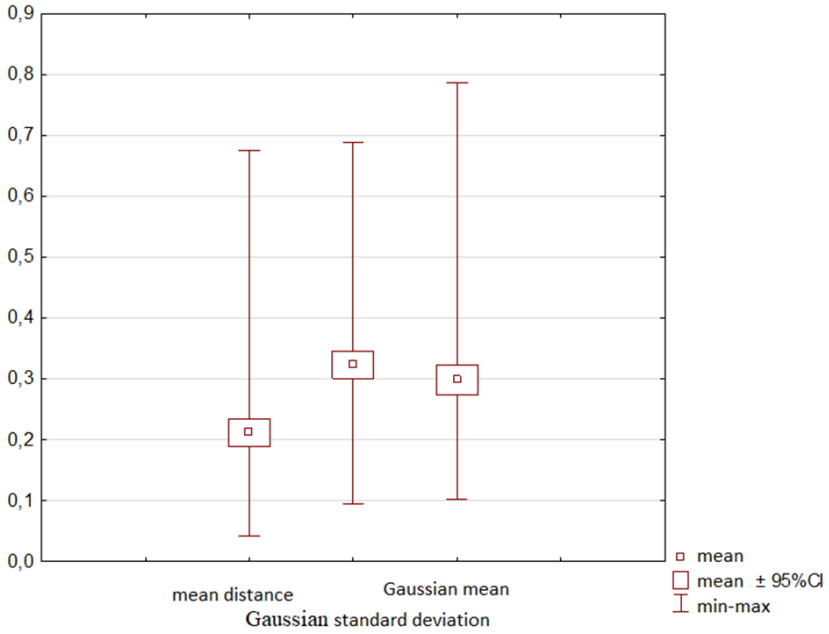

Figure 4. The values of mean distance, standard deviation and Gaussian mean observed in the study

In order to specify whether there is any correlation between the segmentation threshold and the accuracy of CBCT image registration with respect to an optical scan and to determine the optimal segmentation threshold, a number of polynomial regression analyses were performed. Due to the expected nature of the dependency (possibility of an optimal segmentation threshold), the linear and square components were taken into account in the regression analysis. The segmentation threshold was introduced as an independent variable, while the following parameters were selected as dependent variables of the measure of CBCT image matching measures, i.e. mean distance, Gaussian mean and standard deviation from the Gaussian mean.

In the case of mean distance, the proposed model did not significantly explain the variation of the dependent variable: $F(2;105) = 0.16$; $p = 0.856$; $R^2 = 0.002$. This means that the segmentation threshold was not significantly associated with the mean distance. The regression coefficients and the correlation between the two values are shown in Table 3, Figure 5.

Table 3. Factors of regression analysis predicting mean distance on the basis of segmentation threshold

	B	*SE*	*t*	*p*	β
(Constant)	0.26	0.30	0.86	0.391	
Segmentation threshold	0.00	0.00	-0.20	0.838	-0.186
(Segmentation threshold)^2	0.00	0.00	0.26	0.796	0.235

B – regression factor; SE – standard error; t – test statistic; p – statistical significance; β – standardised regression factor.

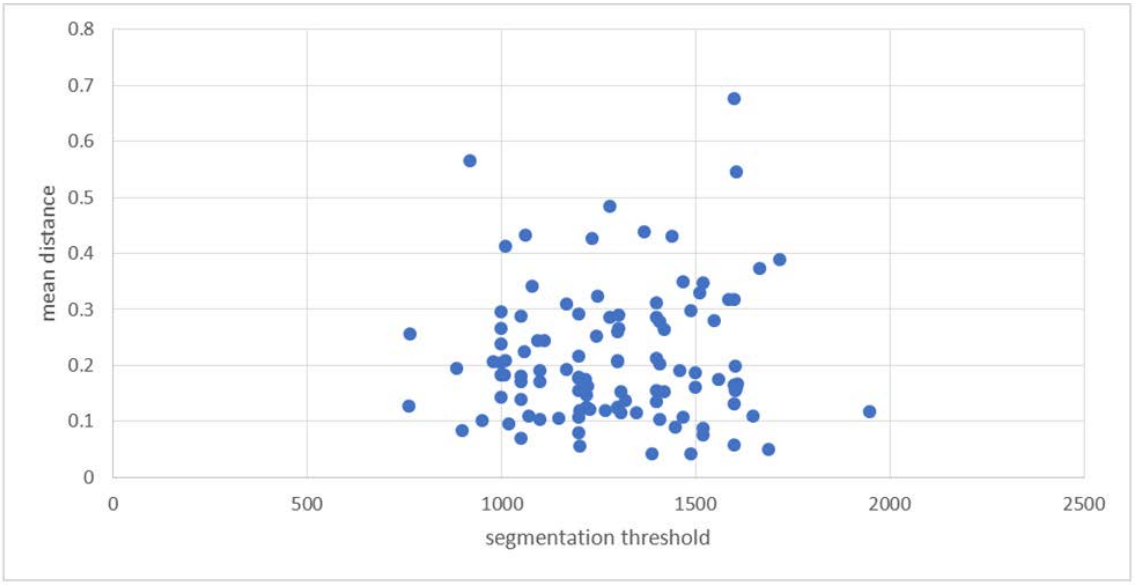

Figure 5. The correlation between the segmentation threshold and the mean distance

Table 4. Factors of regression analysis predicting the Gaussian mean on the basis of segmentation threshold

	B	*SE*	*t*	*p*	β
(Constant)	0.34	0.32	1.08	0.285	
Segmentation threshold	0.00	0.00	-0.18	0.854	-0.167
(Segmentation threshold)^2	0.00	0.00	0.23	0.818	0.209

B – regression factor; *SE* – standard error; *t* – test statistic; *p* – statistical significance; β – standardised regression factor.

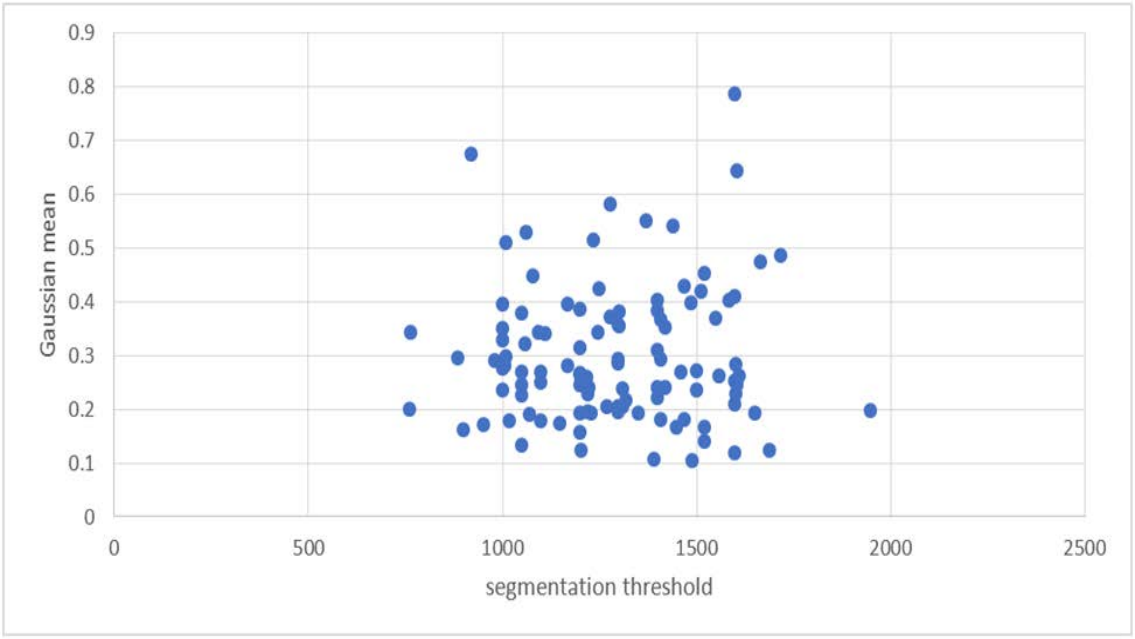

Figure 6. The correlation between the segmentation threshold and the Gaussian mean

Table 5. Factors of regression analysis predicting the Gaussian standard deviation on the basis of segmentation threshold

	B	*SE*	*t*	*p*	β
(Constant)	0.57	0.29	1.97	0.052	
Segmentation threshold	0.00	0.00	-0.73	0.470	-0.652
(Segmentation threshold)^2	0.00	0.00	0.59	0.558	0.528

B – regression factor; *SE* – standard error; *t* – test statistic; *p* – statistical significance; β – standardised regression factor.

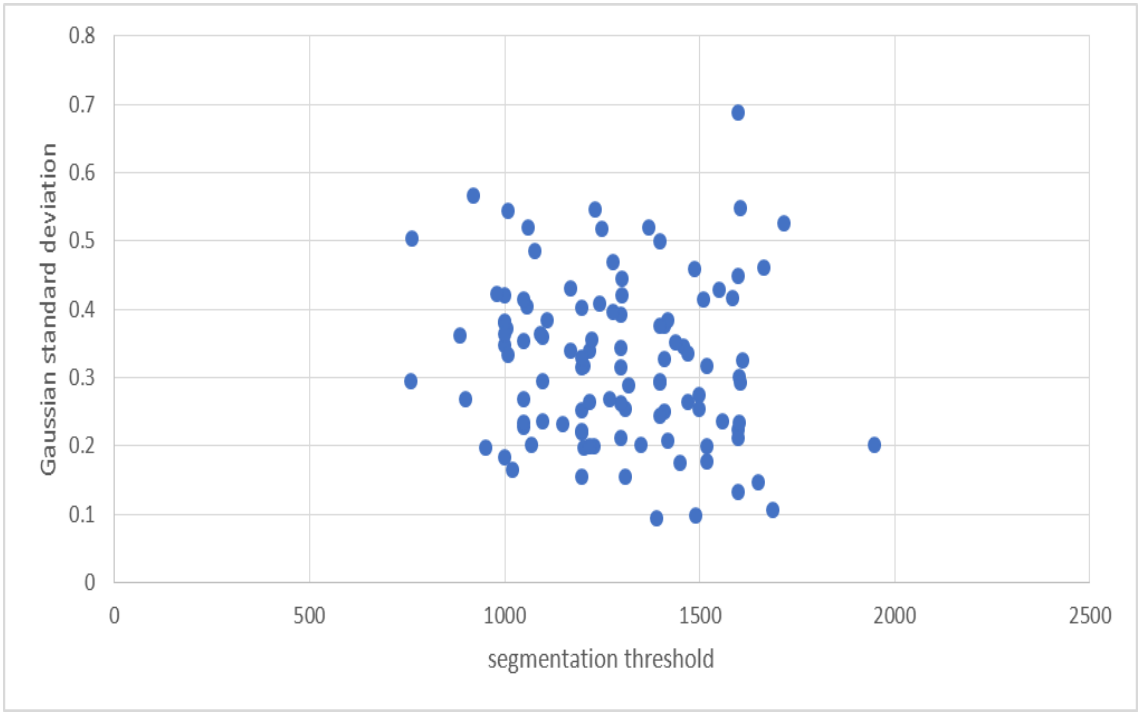

Figure 7. The correlation between the segmentation threshold and the Gaussian standard deviation

Also in the case of the Gaussian mean the proposed model did not explain significantly the variation of the dependent variable: F(2;105) = 0.11; p = 0.894; R2 = 0.002. This means that the segmentation threshold was not significantly associated with the Gaussian mean (Table 4, Figure 6).

The segmentation threshold was also not associated with the standard deviation from the Gaussian mean: $F(2;105) = 1.03$; $p = 0.359$; $R^2 = 0.019$. (Table 5, Figure 7).

4. Discussion

CC software was used in this study to compare objects as separate point clouds. Converting the grid of an object into a point cloud enabled the use of vector analysis (scalar fields) and imaging of the results in the form of colourful graphs and illustrations (Figure 8). First, the Interactive Transformation Tool was used, followed by the ICP algorithm as the 'Fine registration tool (ICP)', which allowed the authors to register almost identical grids of objects. The mean distance (reflecting the measured distances) and the Gaussian mean with its standard deviation (as a result of statistical processing of registration accuracy) were obtained based on the conducted calculations. On the basis of the analysis presented in Table 2, the mean distance (M=0.21) was smaller than the Gaussian mean (M=0.30) by 90 microns, which proves that in reality one should take into account an actual error of registration totalling approximately 300 microns. This was also confirmed by the high value of standard deviation from the Gaussian mean (M=0.32), which could have been caused by actual differences in the geometry of the examined grids and the artefacts of segmented objects from CBCT images remaining after manual processing (Figure 9). Numerous artefacts were caused by the heterogeneous thickness of the enamel layer and the presence of different materials used for tooth reconstruction. The authors hereof used one study performed with another device to visually compare the quality of segmented images from two different sources. This comparison showed that the segmented surfaces compared to the alternative device proved to be much smoother, with fewer artefacts (Figure 10). Therefore, it was possible to conclude that CBCT image quality had an impact on the quality of segmentation and, consequently, on the high value of standard deviation. The 3D image analysis demonstrated that the surface of the optical scan (reference scan) interweaved (permeated) with the occlusal surface of the CBCT scan at different thresholds of segmentation, which from the clinical point of view should be considered a cause for concern, because the geometry of the object from the CBCT study shrinks at the increasing threshold of segmentation. However, the final result of segmentation was also affected by the heterogeneity of grayscale representation, which may compensate for this shrinkage [24,25,26]. From a statistical point of view, it is worth noting that the registration of images can also be possible at different thresholds of segmentation, which may be clinically used to eliminate strong artefacts.

Furthermore, the statistical analysis revealed that there was no statistical relationship between the examined parameters (mean distance, Gaussian mean, standard deviation) and the segmentation threshold (Table 3, Table 4, Table 5, Figure 5, Figure 6, Figure 7). From the clinical point of view, one can conclude that with the statistical error of registration (Gaussian mean=0.3) the adopted segmentation thresholds give statistically equivalent results, which allows to use manual segmentation of structures characterised by varied radiological density. Therefore, it can be assumed that manual segmentation can be used and should be performed taking into account the clinical situation and the quality of CBCT imaging.

In the light of the above the accuracy of registration in clinical settings might be improved by selecting surface fragments free of artefacts caused by the presence of different materials used for tooth reconstruction (such as composites, metals, ceramics), which has not been investigated in this study. It is worth noting that a 0.3 registration error applies to full arches and is likely to be smaller for shorter distances, which however requires additional research. From the prosthetic point of view, the error value of 0.3 is significant, but it allows for the initial design of the course of the occlusal plane and may be a starting point for the clarification of its geometry by other methods.

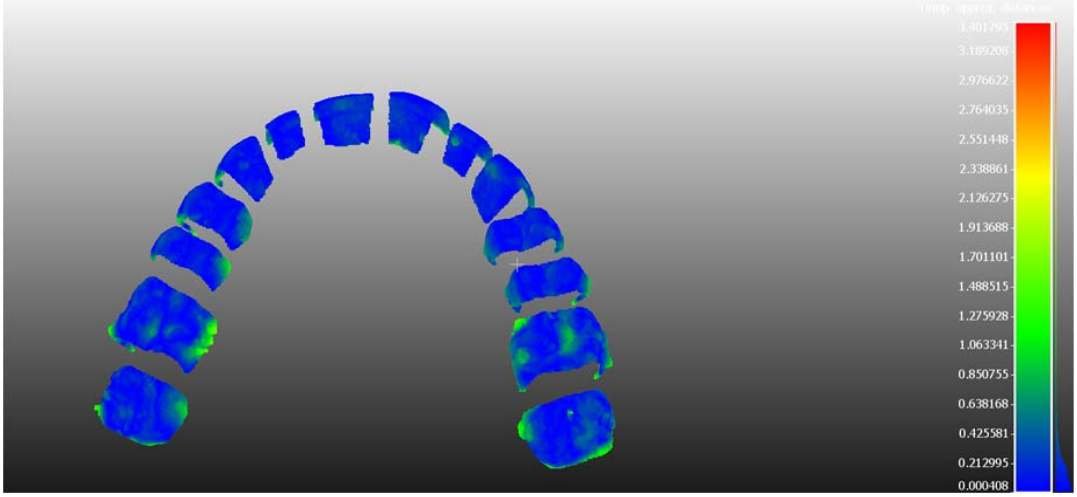

Figure 8. An example of an object composed of a point cloud created after performing statistical calculations which shows the average distances between the examined

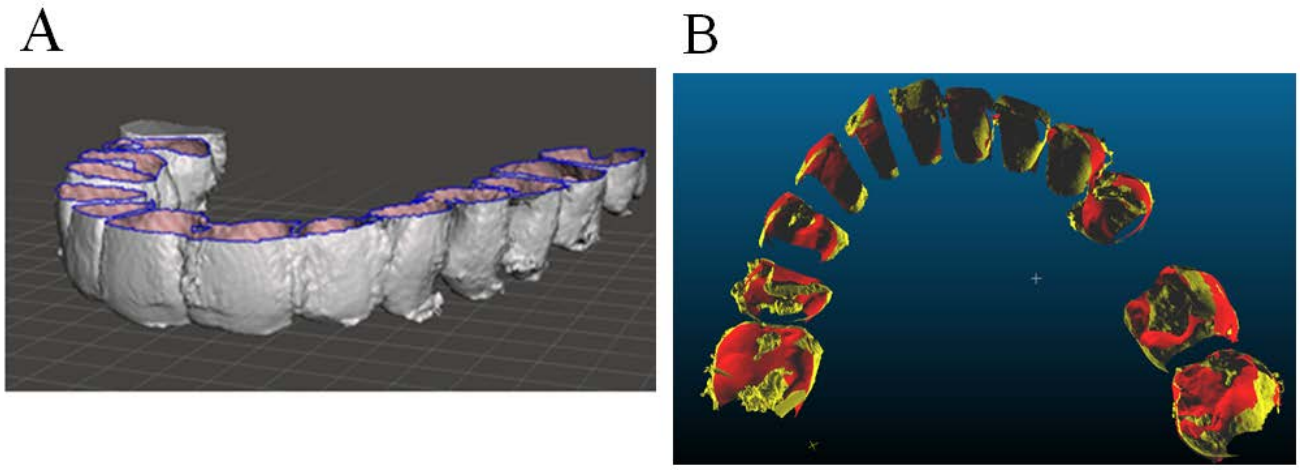

Figure 9. Visible artefacts left after segmentation and processing of models: A – STL model developed based on CBCT scan (Meshmixer); B – red model-optical scan, yellow STL model based on CBCT scan (CloudCompare)

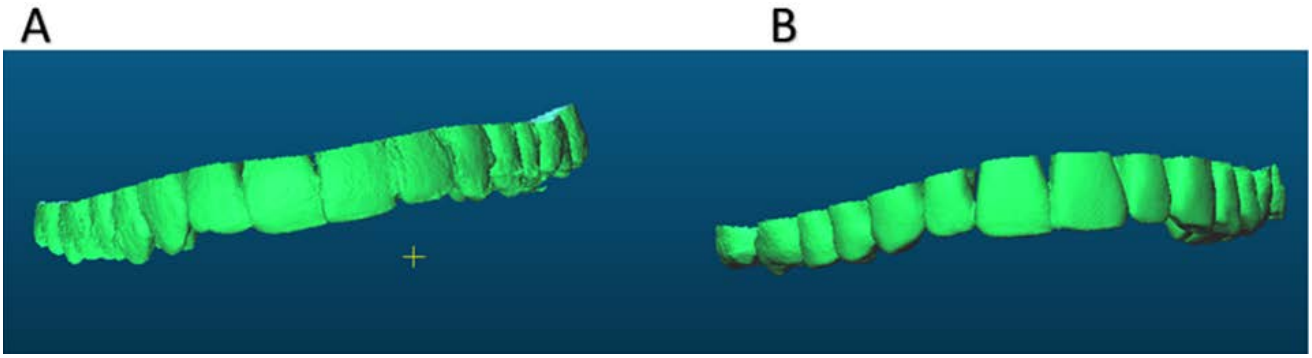

Figure 10. The impact of CBCT imaging quality on the smoothness of segmented surfaces. Two images taken by different devices arranged side by side. A – Vatech Pax-I 3d Green Corea; B – PaxReve3D Corea

5. Conclusions

The results of this study showed that registration accuracy of CBCT data and full arch optical scans can be accepted and successfully applied under clinical conditions with the statistically calculated error of 300 microns. However, it should be taken into account whether such an error is or is not acceptable in a given situation and with regard to a specific clinical procedure.

References

[1] Honey OB, Scarfe WC, Hilgers MJ, Klueber K, Silveira AM, Haskell BS, Farman AG. Accuracy of cone-beam computed tomography imaging of the temporomandibular joint: Comparisons with panoramic radiology and linear tomography. *American Journal of Orthodontics and Dentofacial Orthopedics* 2007 Oct; 132(4): 429-38.

[2] Lascala CA, Panella J, Marques MM. Analysis of the accuracy of linear measurements obtained by cone beam computed tomography (CBCT-NewTom). *Dentomaxillofacial Radiology* 2004 Sep; 33(5): 291-4.

[3] Van Dessel J, Nicolielo LF, Huang Y, Coudyzer W, Salmon B, Lambrichts I, Jacobs R.Accuracy and reliability of different cone beam computed tomography (CBCT) devices for structural analysis of alveolar bone in comparison with multislice CT and micro-CT. *European Journal of Oral Implantology*. 2017; 10(1): 95-105.

[4] Juneja R, Gupta A, Singh S, Kumar V, Role of Cone Beam Computed Tomography in Dentistry. (2016). *Journal of Biosensors, Biomarkers and Diagnostics* 1(1): 1-8.

[5] Prashant P Jaju, Sushma P Jaju, Clinical utility of dental cone-beam computed tomography: current perspectives. *Clinical, Cosmetic and Investigational Dentistry* 2014; 6: 29-43.

[6] Hegde S, Ajila V, Kamath JS, Babu S, Pillai DS, Nair S M. Importance of cone-beam computed tomography in dentistry: An update. *SRM J Res Dent Sci*. 2018; 9: 186-90.

[7] Evain, T., Ripoche, X., Atif, J., & Bloch, I. (2017). Semi-automatic teeth segmentation in Cone-Beam Computed Tomography by graph-cut with statistical shape priors. *2017 IEEE 14th International Symposium on Biomedical Imaging* (ISBI 2017), 1197-1200.

[8] Li Wang, Yaozong Gao, Feng Shi, Gang Li, Ken-Chung Chen, Zhen Tang, James J. Xia, Dinggang Shen, Automated segmentation of dental CBCT image with prior-guided sequential random forests. *Med Phys*. 2016 Jan; 43(1): 336-346.

[9] Schulze, R., Heil, U., Gross, D., Bruellmann, D. D., Dranischnikow, E., Schwanecke, U., & Schoemer, E. (2011). Artefacts in CBCT: a review. *Dento maxillo facial radiology*, 40(5), 265-273.

[10] Fakhar, Hooriyeh Bashizade et al. "Effects of artifact removal on cone-beam computed tomography images." *Dental research journal* vol. 15,2 (2018): 89-94.

[11] Flügge T, Derksen W, Te Poel J, Hassan B, Nelson K, Wismeijer D. Registration of cone beam computed tomography data and intraoral surface scans - Aprerequisite for guided implant surgery with CAD/CAM drilling guides. *Clin Oral Implants Res.* 2017 Sep; 28(9):1113-1118.

[12] Suebnukarn, Siriwan & Haddawy, Peter & Dailey, Matthew & Cao, Dinh. (2008). Interactive Segmentation and Three-Dimension Reconstruction for Cone-Beam Computed-Tomography Images. *NECTEC Technical Journal*. 8. (2008).

[13] Vallaeys K, Kacem A, Legoux H, Le Tenier M, Hamitouche C, Arbab-Chirani R. 3D dento-maxillary osteolytic lesion and active contour segmentation pilot study in CBCT: semi-automatic vs manual methods. *Dentomaxillofac Radiol*. 2015; 44(8).

[14] Mangano F, Gandolfi A, Luongo G, Logozzo S. Intraoral scanners in dentistry: a review of the current literature. *BMC Oral Health*. 2017 Dec 12; 17(1): 149.

[15] Kattadiyil MT, Mursic Z, AlRumaih H, Goodacre CJ. Intraoral scanning of hard and soft tissues for partial removable dental prosthesis fabrication. *J Prosthet Dent.* 2014 Sep; 112(3): 444-8.

[16] Abduo J, Elseyoufi M. Accuracy of Intraoral Scanners: A Systematic Review of Influencing Factors. Eur J *Prosthodont Restor Dent*. 2018 Aug 30; 26(3): 101-121.

[17] Treesh JC, Liacouras PC, Taft RM, Brooks DI, Raiciulescu S, Ellert DO, Grant GT, Ye L. Complete-arch accuracy of intraoral scanners. *J Prosthet Dent*. 2018 Sep; 120(3): 382-388.

[18] Mangano FG, Hauschild U, Veronesi G, Imburgia M, Mangano C, Admakin O. Trueness and precision of 5 intraoral scanners in the impressions of single and multiple implants: a comparative in vitro study. *BMC Oral Health*. 2019 Jun 6; 19(1): 101.

[19] Akyalcin S, Dyer DJ, English JD, Sar C. Comparison of 3-dimensional dental models from different sources: diagnostic accuracy and surface registration analysis. *Am J Orthod Dentofacial Orthop*. 2013 Dec; 144(6): 831-7.

[20] Hyuk-Jin Kwon, Kack-Kyun Kim, Won-Jin Yi. Comparison of digital models generated from three-dimensional optical scanner and cone beam computed tomography. *Journal of Dental Rehabilitation and Applied Science* 2016; 32(1): 60-69.

[21] Flügge T, Derksen W, Te Poel J, Hassan B, Nelson K, Wismeijer D. Registration of cone beam computed tomography data and intraoral surface scans - Aprerequisite for guided implant surgery with CAD/CAM drilling guides. *Clin Oral Implants Res*. 2017 Sep; 28(9): 1113-1118.

[22] Tang T, Liao L, Huang Z, Gu X, Zhang X. Accuracy of the evaluation of implant position using a completely digital registration method compared with a radiographic method. *The Journal of prosthetic dentistry* Dent. 2019 Apr 9.n.pag.

[23] George, D. and Mallery, P. (2010). SPSS for Windows Step by Step*: A Simple Guide and Reference 17.0 Update. 10th Edition*, Pearson, Boston.

[24] van Eijnatten M, Koivisto J, Karhu K, Forouzanfar T, Wolff J. The impact of manual threshold selection in medical additive manufacturing. Int J Comput Assist *Radiol Surg*. 2017 Apr; 12(4): 607-615.

[25] Huotilainen E, Jaanimets R, Valášek J, Marcián P, Salmi M, Tuomi J, Mäkitie A,Wolff J. Inaccuracies in additive manufactured medical skull models caused by the DICOM to STL conversion process. *J Craniomaxillofac Surg*. 2014 Jul; 42(5): e259-65.

[26] van Eijnatten, Maureen & Berger, Ferco & Graaf, Pim & Koivisto, Juha & Forouzanfar, Tymour & Wolff, Jan. (2017). Influence of CT parameters on STL model accuracy. *Rapid Prototyping Journal*. 23.